Optical response of thin amorphous films to infrared radiation

J. Orosco and C. F. M. Coimbra[*]

*Department of Mechanical and Aerospace Engineering, Center for Energy Research, University of California San Diego,
La Jolla, California 92093-0411, USA*

We briefly review the electrical-optical response of materials to radiative forcing within the formalism of the Kramers-Kronig relations. A commensurate set of criteria is described that must be met by any frequency-domain model representing the time-domain response of a real (i.e., physically possible) material. The criteria are applied to the Brendel-Bormann (BB) oscillator, a model that was originally introduced for its fidelity at reproducing the non-Lorentzian peak broadening experimentally observed in the infrared absorption by thin amorphous films but has since been used for many other common materials. We show that the BB model fails to satisfy the established physical criteria. Taking an alternative approach to the model derivation, a physically consistent model is proposed. This model provides the appropriate line-shape broadening for modeling the infrared optical response of thin amorphous films while adhering strictly to the Kramers-Kronig criteria. Experimental data for amorphous alumina (Al_2O_3) and amorphous quartz silica (SiO_2) are used to obtain model parametrizations for both the noncausal BB model and the proposed causal model. The proposed model satisfies consistency criteria required by the underlying physics and reproduces the experimental data with better fidelity (and often with fewer parameters) than previously proposed permittivity models.

I. INTRODUCTION

Determining the frequency domain response, or "permittivity," of materials to electromagnetic forcing is critical to the design and fabrication of optics and electronics [1,2], with applications that include optoelectronics, fiber optics, thin films, optical interference devices (e.g., filters, beam splitters, and mirrors), microelectronics (e.g., integrated circuits), and many other sensing devices [1,3–6]. Closed-form representations of permittivity that are realized in terms of physically meaningful parametrizations (i.e., models) provide the required quantitative interpretation for reproducing experimental data. As a matter of convenience, they also represent a compact and continuous alternative to discrete tabular data. A continuously defined function may be desirable, or even required, for reasons of theoretical compatibility [7–9].

The usual approach to constructing models of this type is to use a sum of basis harmonic oscillators to capture the oscillatory dynamics that underlie the macroscopically observed response. The classical Lorentz harmonic oscillator theory is often found to be insufficient to reproduce the line shapes observed in experiments unless additional, and often unphysical, basis oscillators are added. Thus, efforts at improving these models often involve formulating a more complete oscillator to fit the experimentally observed features. This phenomenological type of model development is frequently undertaken with an entire class of materials in mind [3,10].

Perhaps the most common non-Lorentzian phenomenon observed in the response of real materials is a broadening of the line shape about a known critical point (i.e., resonant frequency). Peak broadening of this type is typically observed experimentally to be somewhere between that of classical Lorentzian and Gaussian profiles. Behavior that in many cases more closely resembles Gaussian broadening has been found in a number of material types (e.g., glasses, metals, and semiconductors). [3,11–13].

A class of models that is commonly leveraged for its utility in reproducing complex-valued, nonclassically broadened line shapes employs Brendel-Bormann (BB) oscillators [3,4,10,14]. The BB oscillator results from a simple convolution product of the classical complex damped Lorentz oscillator with the Gaussian exponential. Unfortunately, as is demonstrated in this work, models utilizing the BB oscillator fail the Kramers-Kronig criteria for physical consistency of material response functions and do not generally represent a corresponding real-valued, causal time-domain response. In this work, we define an oscillator that provides better results for line-shape broadening with an equivalent number of parameters or fewer while strictly adhering to the established criteria for physical consistency.

The organization of this work is as follows. In the remainder of this section, the pertinent theory surrounding material permittivity is briefly summarized. A concise, relevant discussion surrounding causality and the Kramers-Kronig formalism is presented. The BB model is then introduced and investigated using the Kramers-Kronig criteria. In Sec. II, a Gaussian-Lorentzian oscillator is defined, and a comparative mathematical analysis is given. In Sec. III, models are presented which have been obtained using experimental data for amorphous alumina (Al_2O_3) and amorphous quartz silica (SiO_2). The models are parameterized using both the BB configuration and the proposed configuration. Similarities and differences between the models (and their respective parametrizations) are discussed.

[*]Corresponding author: ccoimbra@ucsd.edu

A. Linear-response theory

In linear optical media, the polarization density (or, simply, the polarization) is an extensive property that describes the bulk macroscopic response of the medium- to low-intensity electromagnetic radiation. The polarization P_i for a homogeneous medium at a given time t is expressed as [15]

$$P_i(t) = \int_{-\infty}^{\infty} G_{ij}(t - t') \, E_j(t') \, dt', \tag{1}$$

where G_{ij} is the Green's function tensor representing the material response to arbitrary perturbations in the external electric field E_i. Here we have neglected the local-field correction, an omission that implies no loss of generality within the scope of this work [15]. In cubic media or for isotropic materials, the tensor relations are diagonal in all coordinate systems, so that scalar expressions apply [16]. The displacement field may then be used under a Fourier transform to express the relative permittivity ε of the medium:

$$\varepsilon = 1 + \chi, \tag{2}$$

where $\chi = \chi_e + \chi_d$ is the susceptibility, which corresponds to the Fourier transform of G. The values χ_e and χ_d represent contributions from electronic and dielectric behaviors, respectively.

Over absorptive bands, the relative permittivity is frequency dependent and complex valued (to account for phase loss). For the insulating amorphous materials considered in this work, however, the core electrons in the medium represent a real constant contribution χ_e to the susceptibility, so that defining the real constant $\varepsilon_\infty \triangleq 1 + \chi_e$, the relative permittivity for a medium having L distinct absorptive mechanisms may be written

$$\varepsilon(\nu) = \varepsilon_\infty + \sum_{l=1}^{L} \chi_{d,l}(\nu), \tag{3}$$

where the wave number ν (cm^{-1}) is commonly replaced in the literature with frequency (s^{-1}), angular frequency (rad/s), or energy (eV) as appropriate for the materials or applications.

The complex permittivity is related to the complex refractive index, $\tilde{n} = n + i\,k$:

$$\begin{aligned} \varepsilon &= \tilde{n}^2, \\ &= n^2 - k^2 + i\,2\,n\,k, \end{aligned} \tag{4}$$

so that when the former is known, the latter may always be computed. Here n is the dispersive index, and k is the absorptive index. The absorptive-dispersive indices can be used along with Fresnel's well-known equations to obtain many useful radiative and optical properties, which can, in turn, be used for the application-specific design of materials commonly used in, e.g., optics and microelectronic device fabrication.

B. Kramers-Kronig relations

As briefly reviewed and outlined above, the frequency-dependent permittivity represents the Fourier transform of a material *response* function. For such a function to be physically meaningful, it must obey causality. Within the context of the present discussion, we assume relativistic causality, which implies that a signal cannot propagate faster than the speed of light in a vacuum.

A more formal definition can be given if we consider the scalar form of (1) with a unit impulse $E(t) = \delta(t)$, for which the sifting property of the Dirac-δ function gives $P_\delta(t) = G(t)$. This implies that $G(t)$ is the (impulse) response at time t to the field impulse applied at $t = 0$, so that by the principle of causality, $G(t) = 0 \; \forall \; t < 0$. If G has this property, then the function $\chi(\omega) = \mathcal{F}\{G(t)\}$, where $\mathcal{F}\{\cdot\}$ is the Fourier transform, is causal.

Titchmarsh previously established [17] that this result is equivalent to the requirement that the real and imaginary parts of χ form a Hilbert transform pair. If we further require that the time-domain impulse response be real valued, then the susceptibility must be Hermitian, and the Kramers-Kronig relations (KKRs) hold:

$$\begin{aligned} \chi'(\nu) &= \frac{2}{\pi} \mathcal{P} \int_0^\infty \frac{\overline{\nu}\, \chi''(\overline{\nu})}{\overline{\nu}^2 - \nu^2} \, d\overline{\nu}, \\ \chi''(\nu) &= -\frac{2}{\pi} \mathcal{P} \int_0^\infty \frac{\nu\, \chi'(\overline{\nu})}{\overline{\nu}^2 - \nu^2} \, d\overline{\nu}, \end{aligned} \tag{5}$$

with $\chi' = \mathbb{Re}\{\chi\}$ and $\chi'' = \mathbb{Im}\{\chi\}$. The notation $\mathcal{P}$ implies that, since the integrand in each expression is singular at ν, the Cauchy principal value should be recovered. When modeling directly in the frequency domain, assessing causality of a given model is not always a straightforward endeavor. The KKRs are useful in this regard, and when they are satisfied, they can be leveraged in the experimental setting toward other practical ends.

When evaluating closed-form expressions (i.e., models), it is usually a less tedious exercise to invoke the fundamental assumptions established when deriving the KKRs, which is achieved assuming relativistic causality of a real-valued time domain response function [18,19]: (1) $\chi(\nu)$ is analytic in the upper half plane, (2) $\chi(\nu) \to 0$ as $|\nu| \to \infty$ at least as fast as $1/|\nu|$, and (3) $\chi(\nu)$ is Hermitian. In other words, a function satisfies the KKRs if it satisfies the three preceding items.

The first item is directly related to (and implies) causality. It tells us that a causal function may have no singularities in the upper half complex plane [20]. The second statement is a convergence requirement that arises when forming a contour integral enclosing the upper half plane. Note that we may relax this statement to allow the function to approach a real constant as $|\nu| \to \infty$, in which case the contour integral is still convergent. Under this relaxation, the permittivity fulfills the criteria with the appropriate constant being ε_∞, in accordance with (3). Thus, the criteria are also found in the literature with the second requirement written in this relaxed form [21,22]. The final statement is necessary since the Fourier transform of a function is real valued if and only if the function is Hermitian.

When it is reasonable to do so, the KKRs should be written using the expressions (5) rather than as a Hilbert transform pair. This is because non-Hermitian functions may satisfy the Hilbert transform [21,23]. This subtle, yet important, distinction is a possible source of confusion contributing to the misclassification of some models as KKR consistent [3,10,14] when they are not [22].

C. Brendel-Bormann oscillator

In crystalline materials, phonon absorption in the infrared regime is generally attributed to the existence of Van Hove

singularities in the density of states [24]. These represent points of nondifferentiability (also referred to as critical points) in the reciprocal lattice. Analyses of these materials are typically of a first-principles sort, relying on the crystal structure and periodicity to characterize response dynamics. These include computational methods such as density functional theory [25,26] and analytical methods that parametrize the spatially dispersive effects in terms of the phonon modes [26–28]. The latter methods are useful for resolving optical properties of the medium over frequency-dependent bands.

In many materials, these methods may be insufficient to adequately describe the material responses [3,5,29,30], many of which exhibit a broadened, non-Lorentzian character. These include (among others) amorphous media and glasses [10–12,31], semiconductors [5,13], and metals/conductors [3]. Peak broadening of this kind represents the overlapping time scales of dynamics with a frequency-dependent correlation decay. In the infrared response of amorphous solids, this behavior arises primarily as a result of phonon dispersion in the complex lattice geometries, which lack long-range order [32]. Over longer distances, the lattice behaves as a disordered N-body dynamic filter (N is very large), whose macroscopic output is the observed broadening. Thus, a top-down approach to modeling permittivity in these scenarios is a logical one.

One model that has been generally well received since its introduction nearly three decades ago is the BB oscillator [10]. The model was originally introduced as a phenomenological approach to modeling the non-Lorentzian broadening often observed in the infrared response of thin, solid, amorphous films. It is given by the convolution

$$\chi_{BB}(\nu) \triangleq \int_{-\infty}^{\infty} \chi_G(y - \nu_0)\, \chi_L(\nu;\, y)\, dy, \tag{6}$$

where

$$\chi_G(\nu_0) \triangleq \frac{1}{\sqrt{2\pi}\,\sigma} \exp\left[-\left(\frac{\nu_0}{\sqrt{2}\,\sigma}\right)^2\right] \tag{7}$$

represents a Gaussian decay applied to the complex damped harmonic oscillator (CDHO) profile

$$\chi_L(\nu;\, \nu_0) \triangleq \frac{\nu_p^2}{\nu_0^2 - \nu^2 - i\,\gamma\,\nu}, \tag{8}$$

where ν_p is the plasma frequency, γ is the Lorentz broadening parameter, σ is the Gaussian broadening parameter, and ν_0 represents the Lorentzian resonant frequency.

The standard closed-form expression for the evaluation of the convolution in (6) is given in the literature as [3,14]

$$\chi_{BB}(\nu) = \frac{i\,\nu_p^2}{\sqrt{8}\,\sigma\,a}\left[w\left(\frac{a - \nu_0}{\sqrt{2}\,\sigma}\right) + w\left(\frac{a + \nu_0}{\sqrt{2}\,\sigma}\right)\right], \tag{9}$$

where $w(z) \triangleq \exp(-z^2)\,\mathrm{erfc}(-i\,z)$ is the Faddeeva function and $a = a' + i\,a''$ is defined such that $a'' > 0$, with

$$a' = \frac{\nu}{\sqrt{2}}\{[1 + (\gamma/\nu)^2]^{1/2} + 1\}^{1/2},$$

$$a'' = \frac{\nu}{\sqrt{2}}\{[1 + (\gamma/\nu)^2]^{1/2} - 1\}^{1/2}. \tag{10}$$

Note that this is mathematically identical to the closed-form expression originally given by Brendel and Bormann [10],
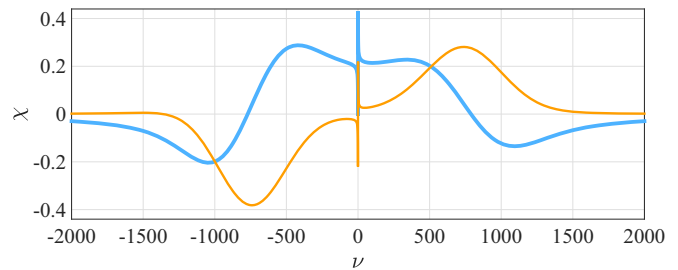

FIG. 1. BB oscillator. The real (thick blue line) and imaginary (thin orange line) parts of the BB oscillator with $\nu_p = 310.83$, $\gamma = 96.49$, $\nu_0 = 816.20$, and $\sigma = 219.9$. The units are cm^{-1}. The parameters are from a multioscillator model for SiO$_2$ (given in full in the results section). Here σ was exaggerated by a factor of 10 to keep the response stable for $\nu < 0$ and to more clearly demonstrate the divergence resulting from the singularity at $\nu = 0$. Note the lack of symmetry (antisymmetry) in the real (imaginary) signal, which indicates the model is not Hermitian. The divergence at $\nu = 0$ indicates the model is not causal.

except that it has been given in terms of the Faddeeva function (primarily for the purposes of computational efficiency).

The closed-form expression in (9) *does not satisfy* the Kramers-Kronig criteria. Indeed, due to an algebraic branch-point singularity at the origin, the model fails the upper half-plane holomorphism requirement of Titchmarsh's theorem [17] and is therefore *not generally causal*. This singularity is due to the parameter a in the denominator of the leading fractional term. The model also fails the parity requirement imposed by the Kramers-Kronig criteria, which is necessary for the signal to correspond to a real-valued time-domain response. These issues are examined graphically in Fig. 1.

II. PROPOSED MODEL

In this section, we propose a model that has been developed from the viewpoint that we would like to retain the beneficial broadening feature of the BB model but also adhere strictly to the Kramers-Kronig criteria. We also prefer that the model produce approximately the same line shape about the Lorentz resonance as that achieved by the BB model under identical experimental parameter sets, although this is not a strict requirement. Whenever this can be accomplished, parametrizations utilizing the BB model that already exist within the literature remain approximately valid for the proposed model structure. Last, we require that our model obey the CDHO asymptotics at high and low frequencies.

A. Parity correction

One observes that since (7) is an even real function and (8) is Hermitian, their product is Hermitian. Furthermore, sums of their products are also Hermitian. For this reason, the result of the previous section, that the convolution sum is parity breaking, is somewhat perplexing. We resolve this incongruity presently.

Throughout this work, we assume that the preferred substructure of the oscillator is Lorentzian and that the Gaussian convolution is employed only as a shape function near and about the Lorentz resonance (this interpretation is underscored
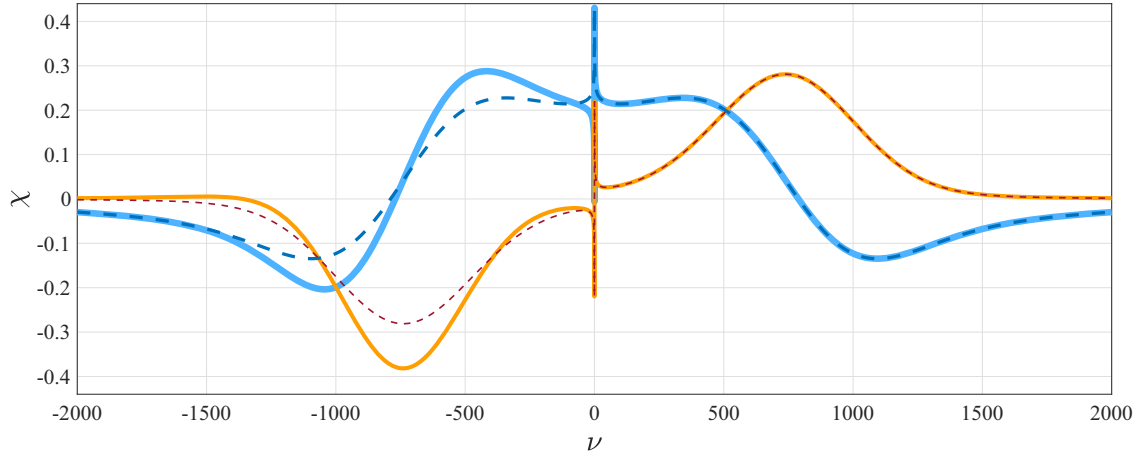
FIG. 2. Parity correction. The same as Fig. 1, except with the addition of the real (thick dashed line) and imaginary (thin dashed line) parts of the model using the corrected expressions in (15), given as a function of wave number (cm^{-1}). The models are identical for $\nu > 0$, but the corrected model retains symmetry (antisymmetry) in the real (imaginary) signals for $\nu < 0$. Near $\nu = 0$, both models diverge, but the corrected model does so in a manner consistent with the even (odd) character of the real (imaginary) signal. This demonstrates that the divergence and parity-breaking issues are independent. In other words, the Fourier transform of the parity-corrected model will be real valued, but it will not generally be causal.

by the ν independence of χ_G). With this in mind, we prefer the form of the convolution given by the change of variables $x \triangleq y - \nu_0$ and leading to

$$\chi(\nu) \triangleq \int_{-\infty}^{\infty} \chi_G(x)\, \chi_L(\nu; x + \nu_0)\, dx, \qquad (11)$$

which removes the ν_0 dependence from the integration limits (i.e., centers the convolution on the CDHO, rather than on $\nu = 0$). Now

$$\chi_L(\nu; x + \nu_0) = \frac{\nu_p^2}{x^2 + 2x\nu_0 + \nu_0^2 - \nu^2 - i\gamma\nu}$$

$$= \frac{\nu_p^2}{(x - p_+)(x - p_-)}$$

$$= \frac{\nu_p^2}{2\alpha}\left(\frac{1}{x - p_+} - \frac{1}{x - p_-}\right), \qquad (12)$$

where $p_\pm \triangleq \pm\alpha - \nu_0$ and $\alpha \triangleq \sqrt{\nu^2 + i\gamma\nu}$. Then

$$\chi(\nu) \triangleq \frac{\nu_p^2}{2\sqrt{2\pi}\,\sigma\,\alpha}(I_+ - I_-), \qquad (13)$$

with

$$I_\pm \triangleq \int_{-\infty}^{\infty} \frac{\exp(-t^2)}{t - z_\pm}\, dt \qquad (14)$$

and where we have defined $t \triangleq x/\sqrt{2}\,\sigma$ and $z_\pm \triangleq p_\pm/\sqrt{2}\,\sigma$. The apparent source of the parity-breaking behavior given by the traditional closed-form expression (9) results from application of a domain-restricted evaluation of improper contour integrals having the same form as (14). The more general result, valid whenever $\mathbb{Im}(z) \neq 0$, is given by

$$I_\pm = i\pi\, w(z_\pm)$$

$$+ \exp(-z_\pm^2)\left[\log(z_\pm) + \log\left(-\frac{z_\pm^*}{|z_\pm|^2}\right) - i\pi\right], \quad (15)$$

where $w(z) \triangleq \exp(-z^2)\operatorname{erfc}(-iz)$ is the Faddeeva function, $\log(z)$ is the complex natural logarithm, z^* denotes the complex conjugate of z, and $|z| = \sqrt{z z^*}$. This result is markedly different from that given by the commonly cited reference of Abramowitz and Stegun [33] [Eq. (7.1.4) therein], which is restricted to cases for which $\mathbb{Im}(z) > 0$. Unfortunately, the domain-restricted result of Abramowitz and Stegun is often misreported in the literature as being a general result [34,35].

If $\nu < 0$, then the expression in square brackets in (15) is generally nonvanishing. The result is that (15) is Hermitian, whereas the traditional expression is not. Since the product of commutable Hermitians is itself Hermitian, (13) will be Hermitian, that is, parity will be preserved, when (15) is used. This is demonstrated in Fig. 2.

B. Singularity removal by approximation

Resolving the zero-frequency divergence issue involves a less direct approach than that used to resolve the parity issue and requires some intuition about the behavior of the component functions involved in (13). Before proceeding, we find it convenient to reexpress our model as

$$\chi(\nu) \triangleq \frac{\nu_p^2}{2\sqrt{2\pi}\,\sigma\,\alpha}[f_w(z_+) - f_w(z_-)], \qquad (16)$$

with

$$f_w(z) = i\pi w(z)$$

$$+ \exp(-z^2)\left[\log(z) + \log\left(-\frac{z^*}{|z|^2}\right) - i\pi\right]. \quad (17)$$

The primary source of the divergence is the factor $1/\alpha$, which is

$$\frac{1}{\alpha} = \frac{1}{(\nu^2 + i\gamma\nu)^{1/2}} = \frac{1}{\nu^{1/2}[\nu - (-i\gamma)]^{1/2}}, \qquad (18)$$

so that the model evidently has two algebraic branch-point singularities, one occurring at $-i\gamma$ and the other at the origin.
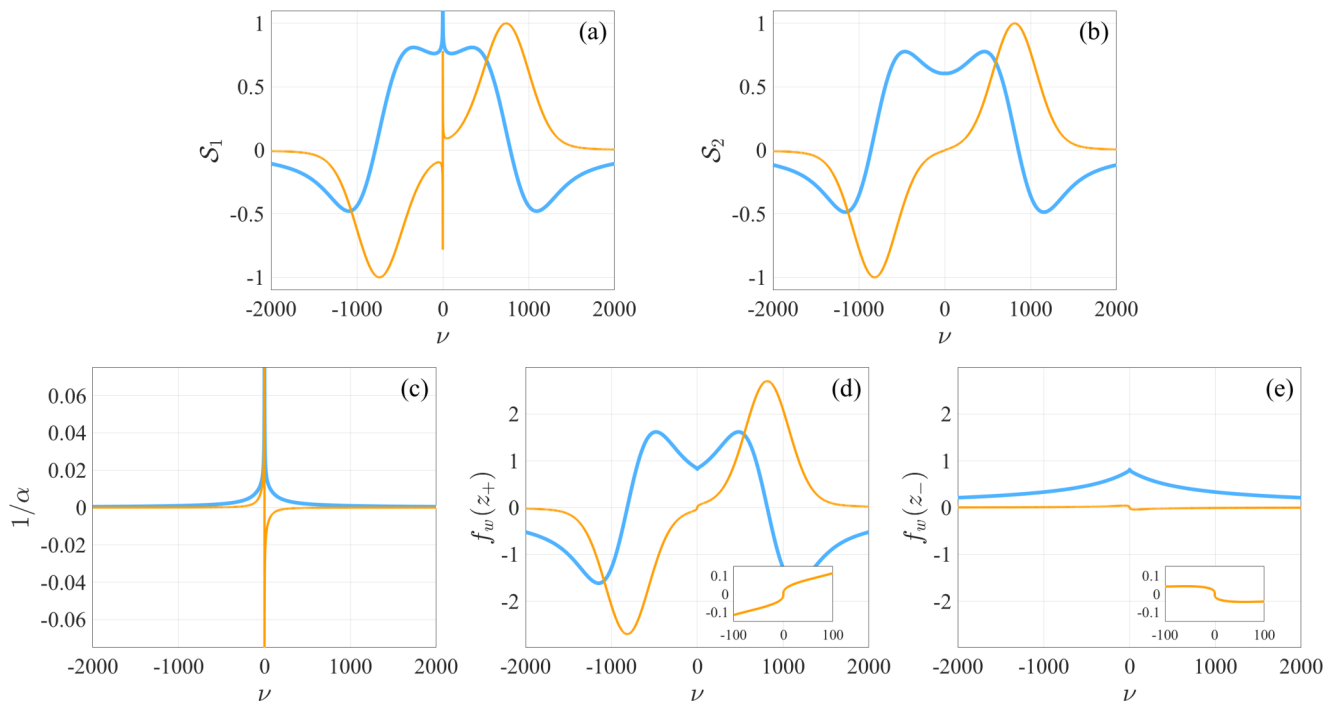
FIG. 3. Singularity removal by approximation. The model parameters are the same as used in Fig. 1. In each plot the thick blue line is the real part, and the thin orange line is the imaginary part, given as a function of wave number (cm^{-1}). The top row gives model shapes (a) before and (b) after singularity removal, with the shapes given by $\mathcal{S}_1 \triangleq (1/\alpha)[f_w(z_+) - f_w(z_+)]$ and $\mathcal{S}_2 \triangleq f_w(z_+) + f_w(z_+)$, respectively. The shape functions have been normalized to the imaginary part for ease of comparison. The bottom row gives the component functions (c) $1/\alpha$, (d) $f_w(z_+)$, and (e) $f_w(z_-)$. The insets of (d) and (e) provide a closer look at the behavior of the imaginary part near the origin. With a sensible recomposition of the component functions, one obtains a continuous (Hermitian) shape where the singularity has been removed. One notes that the maxima of (a) and (b) do not occur at the same wave number. This is a desirable feature that is discussed in detail later.

In fact, the complex logarithm functions of (17) each independently have logarithmic branch-point singularities whenever $z_\pm(\nu) = 0$. Solving for this condition, one finds that the singularities are in the lower half plane as long as $\gamma > 0$, so that the logarithm terms do not violate the criteria. The Faddeeva function, a product of two entire functions, is also entire. When $\gamma > 0$, the corresponding $1/\alpha$ singularity is in the lower half plane, so that this also does not violate the Kramers-Kronig criteria. The branch-point singularity at the origin, on the other hand, does violate the criteria.

In order to deal with the singularity in the $1/\alpha$ factor, we note that this factor contributes negligibly to the overall shape of the model away from $\nu = 0$. Then its primary "purpose" is to provide (multiplicative) support for the overall real and imaginary signals near $\nu = 0$, with the unfortunate side effect of divergence of both in the limit. The term $f_w(z_-)$ mimics this behavior but does so without diverging. However, this term is *subtracted* in (16), so that it *contributes* to the anomalous discontinuous behavior of $f_w(z_+)$ near zero.

Taking all of this into account, it is clear that by reversing the sign (i.e., the behavior) of the $f_w(z_-)$ term and setting $1/\alpha$ to unity, we achieve a line shape that approximates the exact convolution without diverging near $\nu = 0$. The symmetric complimentary behavior of $f_w(z_+)$ and $f_w(z_-)$ is such that a continuous line shape is produced for all ν (including at $\nu = 0$). Furthermore, since we have exchanged a Hermitian term, $1/\alpha$, with another Hermitian term, 1, the parity of the

model is unaffected. This process is perhaps better elucidated graphically, as in Fig. 3.

Due to a scaling difference resulting from these modifications, the model magnitude must be rescaled. The need for rescaling is a desirable one since we can choose this to occur at $\nu = 0$ and require that our model satisfy the asymptotic behavior of the CDHO. In other words, we require that our rescaled model have the property $\chi(\nu = 0) = \chi_L(\nu = 0; \nu_0) = \nu_p^2/\nu_0^2$.

The final proposed model *definition* may be intuitively expressed as

$$\chi(\nu) \triangleq \mathcal{A} \mathcal{S}(\nu), \tag{19}$$

where

$$\mathcal{A} \triangleq \nu_p^2/\nu_0^2 \tag{20}$$

is the amplitude at $\nu = 0$, determined entirely by the plasma frequency and Lorentz resonance, and where

$$\mathcal{S}(\nu) \triangleq \left(\frac{f_w(z_+) + f_w(z_-)}{\chi_0} \right) \tag{21}$$

is a frequency-dependent, dimensionless shape function which is jointly determined by the plasma frequency, the Lorentz resonance, the complex Lorentz damping, and the Gaussian broadening parameter. The function $f_w(z)$ is given in (17), and we recall that $z_\pm \triangleq p_\pm/\sqrt{2}\,\sigma = (\pm\alpha - \nu_0)/\sqrt{2}\,\sigma$. Since the range of α is no longer restricted, we give it the more general
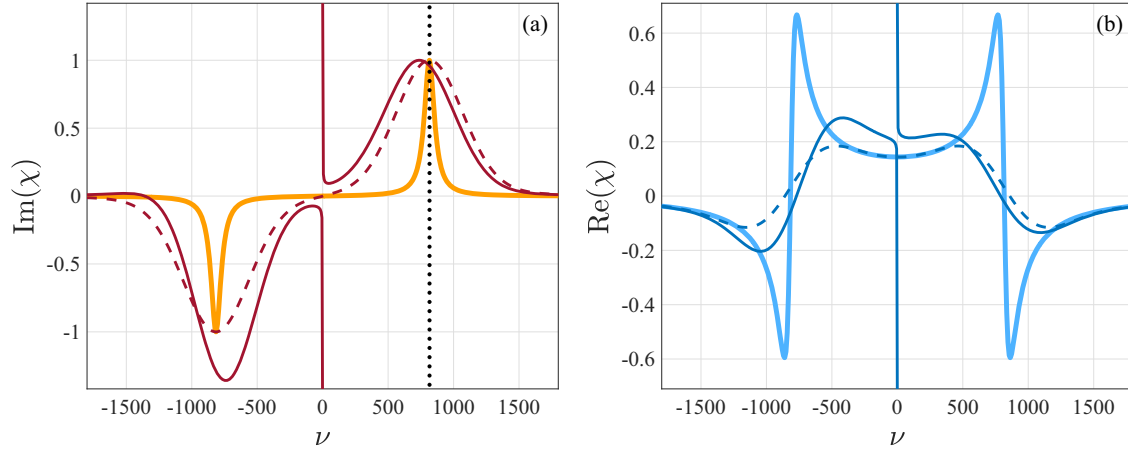
FIG. 4. Comparison with the CDHO profile. (a) Imaginary and (b) real parts of the BB model (thin solid line), the proposed model (thin dashed line), and the CDHO (thick solid line) as a function of wave number (cm^{-1}). The imaginary parts have been normalized by their respective right half-plane maxima for ease of comparison. The model parameters are the same as those used in Fig. 1. The proposed model is asymptotically equivalent to the CDHO (i.e., at $\nu = 0$ and $\nu = \pm\infty$). The frequency of the energy absorption maximum is in nearly perfect agreement with the CDHO. Both have an energy absorption maximum occurring at approximately ν_0, which is indicated in (a) by the vertical dotted line. The proposed model clearly represents a continuous complex function satisfying the KKRs and preserving the relevant characteristics of the underlying classical Lorentz harmonic oscillator theory.

definition $\alpha = \alpha' + i\,\alpha''$:

$$
\begin{aligned}
\alpha' &\triangleq (\nu/2)^{1/2}\,[(\nu^2 + \gamma^2)^{1/2} + \nu\,]^{1/2}, \\
\alpha'' &\triangleq (\nu/2)^{1/2}\,[(\nu^2 + \gamma^2)^{1/2} - \nu\,]^{1/2} + \mu,
\end{aligned}
\tag{22}
$$

where μ is an arbitrarily small constant $0 < \mu \ll 1$ ($\mu = 1/\nu_0$ is a logical choice). Inclusion of μ is necessary for strict analytical adherence to the Kramers-Kronig formalism (its omission has a negligible effect in practice). The normalization parameter is

$$
\chi_0 \triangleq -4\sqrt{\pi}\,D\!\left(-\frac{\nu_0}{\sqrt{2}\,\sigma}\right),
\tag{23}
$$

where $D(z) = (\sqrt{\pi}/2)\,\mathbb{I}\mathrm{m}\{w(z)\}$ is known as Dawson's integral. The parameter χ_0 has been defined so that $\mathcal{S}(\nu = 0) \equiv 1$. In other words, the shape function has unity dc gain.

The resulting proposed model has exactly the properties we set out to achieve: (1) strict Kramers-Kronig consistency, (2) asymptotic equivalence to the CDHO (see Fig. 4), and (3) "tunable" Gaussian broadening. In addition to these points, the model produces a line shape that approximates that of the original BB model under identical parametrizations. For some materials, the two are nearly equivalent. This is demonstrated and discussed in the next section, which contains real material parametrizations for two amorphous materials.

III. RESULTS FOR REAL MATERIALS

For each experimental data set, the model parameters were obtained by minimizing the relative squared error objective,

$$
\begin{aligned}
\mathcal{J}(\theta) \triangleq \frac{1}{2}\sum_{m=1}^{M}\Bigg[&\left(\frac{\varepsilon'(\nu_m;\theta) - \varepsilon'_m}{\varepsilon'_m}\right)^2 \\
&+ \left(\frac{\varepsilon''(\nu_m;\theta) - \varepsilon''_m}{\varepsilon''_m}\right)^2 \Bigg],
\end{aligned}
\tag{24}
$$

where $\varepsilon(\nu;\theta) = \varepsilon'(\nu;\theta) + i\,\varepsilon''(\nu;\theta)$ is the respective model evaluated at a frequency ν given a parameter set θ and $\varepsilon_m \triangleq \varepsilon'_m + i\,\varepsilon''_m$ represents the experimental data defined on some M-sized frequency (or wave number) grid ν_m, $m \in [1, M]$. In practice, one can usually obtain a better fit (or a fit that is tailored to the intended application) by independently weighting (either globally or as a function of frequency) the real and imaginary terms in the objective. We do not weight the objective in this work, choosing instead to uniformly apply (24) in order to provide a more standard basis for comparison.

The objective was minimized with the use of a primal-dual path-following interior-point method [36]. However, users should find no difficulty using their preferred method to fit the model. All models were optimized on a scaled frequency grid in accordance with the findings of Pintelon and Kollár [37]. The optimal parameters were then rescaled to the original grid. The error analysis presented in the following sections was conducted on the true (i.e., rescaled) model parameters.

A. Implementation

When considering the complex Gaussian limit of the model $\gamma \to 0$, one should allow γ to approach some arbitrarily small positive value (say, 10^{-10}) rather than identically zero. This allows the correct sign to be retained when $\nu < 0$ during implementation in a preferred computing environment (e.g., MATLAB), thus retaining the Hermiticity of the model. This represents a valid parameter reduction because the approach to the purely Gaussian limit implies that the oscillator can be replaced with a three-parameter complex Gaussian [13].

The term contributed to (17) by the second term of (15) can occasionally misbehave and produce indeterminate iterates during the optimization routine due to the exponential factor. This should not be viewed as aberrant behavior, but rather as the model structure enforcing the Hermitian requirement of the Kramers-Kronig relations (which might otherwise be
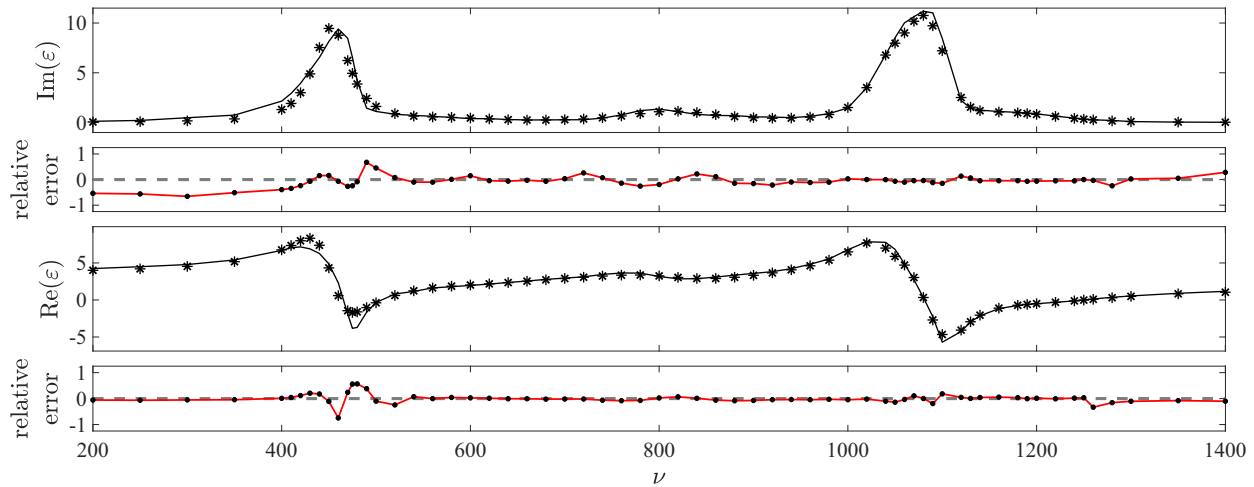
FIG. 5. SiO_2 permittivity as a function of wave number (cm^{-1}). A six-oscillator model is shown, which has been fit to the data of Popov *et al.* [38]. In the model plots, the BB model is indicated by + symbols and the proposed model is indicated by × symbols, so that the ∗ symbol implies consensus. The solid black line indicates the data. In the error plots, the BB model relative error is shown by the solid red line, and the proposed model relative error is shown by the dots. Also shown in the error plots is the relative consensus error (dashed gray line) between the BB model and the proposed model, which is effectively zero everywhere. In each case, the relative errors have been obtained by scaling the true error pointwise by the magnitude of the corresponding experimental data. The parameters for each model are given in Table I.

violated). This occurs when unphysical parameter sets are investigated by the optimization routine. While the authors found this to rarely occur in practice, we address it here for completeness.

The issue arises when $\sigma/\gamma \ll 1$. Users experienced with parameter optimization may take any number of approaches to mitigating the issue should it arise during parameter fitting (e.g., limiting γ to meaningful values) depending on the intended application and the modeling objectives. An approach that will always ensure well-defined iterates is to simply require that $\sigma/\gamma \geqslant \beta$, where we have found $\beta \approx 0.1$ to be a reasonable value. We recall that σ is the Gaussian broadening parameter and γ is the Lorentzian broadening parameter, so that as the model approaches this bound, the line shape approaches the corresponding damped Lorentzian profile (readers may also convince themselves of this fact graphically). In other words, the approach to this bound implies that the Gaussian broadening is unnecessary for the fit and a classical CDHO (requiring one less model parameter) can instead be used without compromising the model fidelity.

Under identical parametrizations, the proposed model approximates the shape of the original BB model. This approximation is very close when σ is somewhat smaller than ν_0 (e.g., $\sigma/\nu_0 \lesssim 0.125$). In practice, this will typically occur when the molecular complexity and/or lattice disorder is relatively low. In the interest of accuracy, a reparameterization should always be obtained when using the proposed model with previously obtained BB parametrizations. However, the advantage of the parameter set similarity is that existing BB parametrizations can be used as initializers for the proposed model structure. When σ/ν_0 meets the approximate requirement above, the optimization algorithm converges quickly (from a BB initializer). In either case, parametrizations of the proposed model are capable of reproducing the fidelity of the BB model while also providing the desirable features previously noted.

When σ is larger, the broadened peak of the proposed model is shifted from that of the BB model. However, the frequency of the proposed model's energy absorption maximum is in nearly perfect agreement with that of the CDHO: both are approximately equal to ν_0. The ultimate goal of the proposed model is to yield a physically interpretable parameterized fit to experimental data (rather than to identically fit an existing model structure). Thus, in these cases the shifted peak of the proposed model is a desirable feature since this means that $E_0 = \hbar \nu_0$ more accurately represents the underlying physics. In other words, the optimized model parameter ν_0 will be in agreement with the experimentally observed critical point when expressed in the parameter space of the proposed model. This is clearly demonstrated in Fig. 4.

B. Silicon dioxide

The data for amorphous silicon dioxide were taken from Popova *et al.* [38], who obtained tabulated values for the refractive index by application of Kramers-Kronig analysis to spectrophotometric reflection measurements. The data were selected since they encompass the broadband infrared response of the material. A more comprehensive study of amorphous SiO_2 is given by Kitamura *et al.*[12], in which a 25-parameter model is obtained for the same data set. Kitamura *et al.*'s model utilizes eight Gaussian-like oscillators to model over the noted spectral range.

Models obtained using the BB oscillator and the proposed oscillator are plotted in Fig. 5 with the corresponding parameters given in Table I. The model performances, as measured by the objective (24), are essentially identical. The parameters for each model are, in most cases equivalent, to within experimental error, with greater differences observed for larger values of the broadening parameter. As noted previously, any oscillator having a corresponding Lorentz damping parameter $\gamma_k = 0$ represents a KKR-consistent complex pure Gaussian oscillator

TABLE I. SiO_2 permittivity model parameters (in units of cm^{-1}). The values marked with a dagger (†) were fixed during optimization (in agreement with the literature [4,10]) and are dimensionless. The last row gives the value of the objective (24) evaluated with the given (minimizing) parameter set. The last column gives the absolute difference of the respective values.

θ	ε_{BB}	ε_P	$|\Delta|$
ε_∞	$2.10^\dagger$	$2.10^\dagger$	0.00
$\nu_{p,1}$	287.63	287.97	0.34
γ_1	0.00	0.00	0.00
$\nu_{0,1}$	1168.76	1166.22	2.54
σ_1	54.29	54.35	0.06
$\nu_{p,2}$	535.58	535.65	0.07
γ_2	0.02	0.00	0.02
$\nu_{0,2}$	1083.50	1083.15	0.35
σ_2	19.37	19.38	0.01
$\nu_{p,3}$	554.23	554.26	0.03
γ_3	39.22	39.23	0.01
$\nu_{0,3}$	1044.57	1044.44	0.13
σ_3	11.34	11.34	0.01
$\nu_{p,4}$	310.83	310.97	0.13
γ_4	96.49	96.53	0.05
$\nu_{0,4}$	816.20	815.60	0.60
σ_4	21.99	21.95	0.03
$\nu_{p,5}$	90.73	90.87	0.14
γ_5	0.19	0.00	0.19
$\nu_{0,5}$	586.45	583.95	2.50
σ_5	38.19	38.31	0.12
$\nu_{p,6}$	430.08	430.16	0.08
γ_6	36.81	36.81	0.00
$\nu_{0,6}$	453.13	452.97	0.16
σ_6	8.51	8.51	0.00
$\mathcal{J}(\theta)$	2.54	2.54	0.00

approximation, which is a three-parameter oscillator. Thus, the proposed model is obtained utilizing only six oscillators (with three of these being of the three-parameter type) and with only 22 parameters.

C. Alumina

Data for alumina (amorphous Al_2O_3) were taken from Eriksson *et al.* [39,40]. Thin-film samples were prepared using electron-beam evaporation with substrate temperatures reaching $\approx$323 K ($\approx$50 °C). The dielectric response was then obtained from spectrophotometric reflectance and transmittance measurements. This material was chosen specifically to contrast the silicon dioxide data. The greater number of degrees of freedom (resulting from the greater molecular complexity), when filtered through the lattice disorder, yields a greater characteristic broadening (resulting from the larger spectrum of dynamics time scales). This is observed in the experimental data of Fig. 6 and is also reflected in the model parameters of Table II. The greater part of the increase in broadening (relative to the silicon dioxide data) can likely be attributed to a greater degree of lattice disorder resulting from the substrate deposition method. Due to the larger relative values realized by each σ_k, there is a significant difference between the parameter sets for the BB model and the proposed model. Regardless, the two models obtain approximately the same minimizing value for the objective (24), indicating equivalent model fidelity. The proposed model is obtained in 11 parameters (with two of the oscillators being of the three-parameter type).

D. General remarks on the models

Each of the foregoing models utilizing the proposed oscillator represents a response function for a material that can physically exist in nature, whereas those utilizing the physically inconsistent oscillator do not. It has been shown that
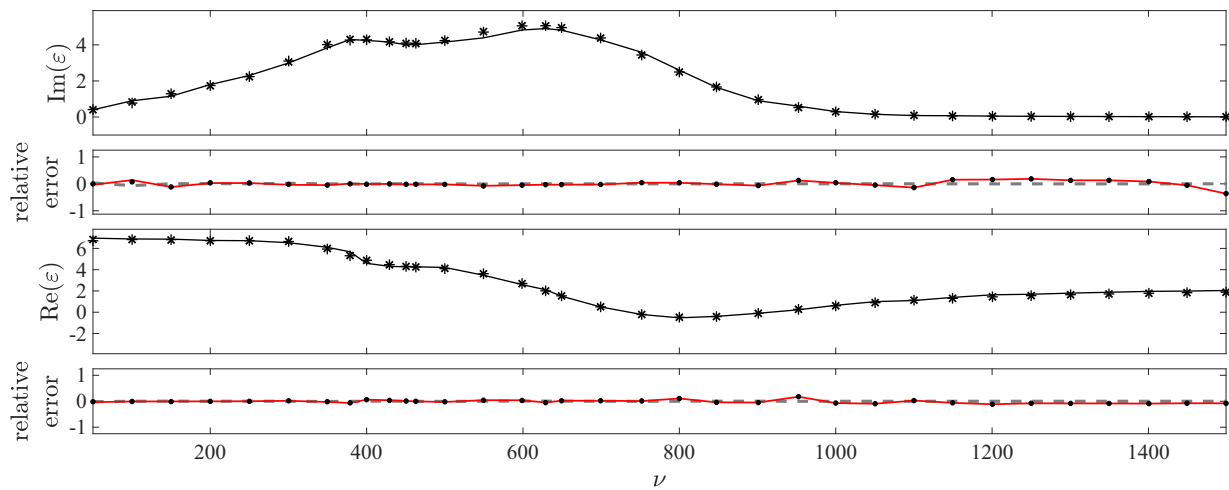

FIG. 6. Al_2O_3 permittivity as a function of wave number (cm^{-1}). A three-oscillator model is shown, which has been fit to the data of Eriksson *et al.* [39,40]. In the model plots, the BB model is indicated by + symbols, and the proposed model is indicated by × symbols, so that the ∗ symbol implies consensus. The solid black line indicates the data. In the error plots, the BB model error is shown by the solid red line, and the proposed model error is shown by the dots. Also shown in the error plots is the consensus error (dashed gray line) between the BB model and the proposed model, which is effectively zero everywhere. In each case, the relative errors have been obtained by scaling the true error pointwise by the magnitude of the corresponding experimental data. The parameters for each model are given in Table II.

TABLE II. Al_2O_3 permittivity model parameters (in units of cm^{-1}). The values marked with a dagger (†) were fixed during optimization (in agreement with the literature [39]) and are dimensionless. The last row gives the value of the objective (24) evaluated with the given (minimizing) parameter set. The last column gives the absolute difference of the respective values.

θ	ε_{BB}	ε_P	$|\Delta|$
ε_∞	2.40†	2.40†	0.00
$\nu_{p,1}$	897.75	917.08	19.34
γ_1	35.41	36.02	0.61
$\nu_{0,1}$	649.35	620.19	29.16
σ_1	142.96	144.27	1.31
$\nu_{p,2}$	329.74	237.05	92.70
γ_2	0.01	0.00	0.01
$\nu_{0,2}$	374.76	372.08	2.68
σ_2	70.41	58.43	11.98
$\nu_{p,3}$	181.53	372.50	190.97
γ_3	0.01	0.00	0.01
$\nu_{0,3}$	223.38	268.47	45.09
σ_3	74.93	139.26	64.33
$\mathcal{J}(\theta)$	0.25	0.24	0.01

the proposed model accurately reproduces the experimental data with at least the same fidelity as the BB model. However, although the near-zero frequency response may not be represented in a given set of data, the singularity in the BB oscillator (demonstrated in Figs. 1 and 4), which implies noncausality, precludes its use in other theoretical frameworks where the response over all frequencies [i.e., $\omega \in (-\infty, \infty)$] is important.

For example, a time-domain analysis of a frequency-dependent material involves Maxwell's equations and utilizes the material's response (i.e., Green's) function. This is known as the finite-difference time-domain method [41]. The material's Green's function is, of course, the inverse Fourier transform of the susceptibility conducted *over all frequencies*. No noncausal material can be expected to produce accurate results when used with such an analysis. Furthermore, any model that is not Hermitian will have a time-domain response function that is generally complex valued and invalid. These issues are irrespective of the experimental data and are therefore also true of the preceding silicon dioxide and alumina models that utilize the BB configuration.

As previously discussed, the proposed model preserves the underlying classical Lorentz harmonic oscillator theory, which is not the case for models such as the critical-point model [7,9] and those generated by Kramers-Kronig construction [35]. The continuous, closed-form functional definition is also an attractive alternative to models utilizing interim extraction of the real parts of auxiliary functions [35], to those utilizing approximate Gaussian quadrature [42], and to those having a limited range of applicability and a limited capability to reproduce the full range of Gaussian character [5,22]. This last point is important because it provides the structural flexibility needed in order to identify (during the model optimization procedure) cases where a parameter reduction is possible by implementation of a purely Gaussian profile.

IV. CONCLUSIONS

The general theory for the response of materials to electromagnetic forcing, when discussed within the context of physically meaningful models, gives rise to the Kramers-Kronig relations. The KKRs are criteria that must be met by a model representing the optical response of a real (i.e., physically possible) material. The criteria are discussed and applied to the Brendel-Bormann model, a model that is frequently used to capture the nonclassical peak broadening observed in many material types (e.g., glasses, metals, and semiconductors). We show that the BB model fails to satisfy these criteria in two independent respects: (1) it is not generally causal, and (2) it does not generally represent a real-valued time-domain response (i.e., its inverse Fourier transform is generally complex valued).

By way of an alternative derivation, we arrived at a consistent model that provides the same fundamental benefits offered by the BB model, Gaussian broadening of a complex damped harmonic oscillator, while adhering strictly to the KKRs. Furthermore, the proposed model is asymptotically equivalent to the CDHO at high and low frequencies. The proposed model has absorption spectrum maxima that occur at frequencies nearly identical to that of the corresponding CDHO's absorption spectrum maxima (near the Lorentz resonance frequencies), whereas the maxima for the BB model may occur at significantly different frequencies.

Parameterizations have been obtained for amorphous alumina (Al_2O_3) and amorphous quartz silica (SiO_2) using both the noncausal BB model and the proposed causal model. The results indicate that the two model types have similar parametrizations for moderate peak broadening. When greater molecular complexity and increased lattice disorder result in more substantial broadening, the resulting parametrizations differ significantly, with the model proposed in this work yielding better agreement with the underlying classical Lorentz harmonic oscillator theory. The proposed model reproduces or exceeds the fidelity of the BB model (as quantified by objective minimization), requiring either the same number or fewer parameters to do so.

[1] D. Franta, D. Nečas, and I. Ohlídal, Appl. Opt. **54**, 9108 (2015).

[2] G. E. Jellison, Jr. and F. A. Modine, Appl. Phys. Lett. **69**, 371 (1996).

[3] A. D. Rakić, A. B. Djurišić, J. M. Elazar, and M. L. Majewski, Appl. Opt. **37**, 5271 (1998).

[4] J. Kischkat, S. Peters, B. Gruska, M. Semtsiv, M. Chashnikova, M. Klinkmüller, O. Fedosenko, S. Machulik, A. Aleksandrova, G. Monastyrskyi, Y. Flores, and W. T. Masselink, Appl. Opt. **51**, 6789 (2012).

[5] C. C. Kim, J. W. Garland, H. Abad, and P. M. Raccah, Phys. Rev. B **45**, 11749 (1992).

[6] D. J. Goldie, A. V. Velichko, D. M. Glowacka, and S. Withington, J. Appl. Phys. **109**, 084507 (2011).

[7] A. Vial and T. Laroche, J. Phys. D **40**, 7152 (2007).

[8] E. A. Muljarov and W. Langbein, Phys. Rev. B **93**, 075417 (2016).

[9] H. S. Sehmi, W. Langbein, and E. A. Muljarov, Phys. Rev. B **95**, 115444 (2017).

[10] R. Brendel and D. Bormann, J. Appl. Phys. **71**, 1 (1992).

[11] D. D. S. Meneses, M. Malki, and P. Echegut, J. Non-Cryst. Solids **352**, 769 (2006).

[12] R. Kitamura, L. Pilon, and M. Jonasz, Appl. Opt. **46**, 8118 (2007).

[13] A. D. Rakić and M. L. Majewski, J. Appl. Phys. **80**, 5909 (1996).

[14] *Semiconductor Terahertz Technology: Devices and Systems at Room Temperature Operation*, edited by L. E. G. M. Guillermo Carpintero, H. L. Hartnagel, S. Preu, and A. V. Räisänen (Wiley, Chichester, UK, 2015).

[15] F. Wooten, *Optical Properties of Solids* (Academic, New York, 1972).

[16] V. Lucarini, K.-E. Peiponen, J. J. Saarinen, and E. M. Vartiainen, *Kramers-Kronig Relations in Optical Materials Research* (Springer, Berlin, 2005).

[17] E. C. Titchmarsh, *Introduction to the Theory of Fourier Integrals*, 2nd ed. (Clarendon, Oxford, 1962).

[18] R. de L. Kronig, J. Opt. Soc. Am. **12**, 547 (1926).

[19] M. H. A. Kramers, *Atti del Congresso Internazionale dei Fisici* (N. Zanichelli, Bologna, 1927), Vol. 2, pp. 545–557.

[20] S. Lang, *Complex Analysis*, 4th ed. (Springer, New York, 1999).

[21] C. D. Keefe, J. Mol. Spectrosc. **205**, 261 (2001).

[22] G. Cataldo and E. J. Wollack, Proc. SPIE **9914**, 99142W (2016).

[23] K.-E. Peiponen and E. M. Vartiainen, Phys. Rev. B **44**, 8301 (1991).

[24] L. Van Hove, Phys. Rev. **89**, 1189 (1953).

[25] M. Mikami, S. Nakamura, O. Kitao, and H. Arakawa, Phys. Rev. B **66**, 155213 (2002).

[26] S. Schöche, T. Hofmann, R. Korlacki, T. E. Tiwald, and M. Schubert, J. Appl. Phys. **113**, 164102 (2013).

[27] F. Gervais and B. Piriou, Phys. Rev. B **10**, 1642 (1974).

[28] J. J. Hopfield and D. Thomas, Phys. Rev. **132**, 563 (1963).

[29] Z. H. Stachurski, Materials **4**, 1564 (2011).

[30] T. Egami, V. Levashov, J. Morris, and O. Haruyama, Metall. Mater. Trans. A **41**, 1628 (2010).

[31] J. Leng, J. Opsal, H. Chu, M. Senko, and D. Aspnes, Thin Solid Films **313–314**, 132 (1998).

[32] H. W. Sheng, W. K. Luo, F. M. Alamgir, J. M. Bai, and E. Ma, Nature (London) **439**, 419 (2006).

[33] *Handbook of Mathematical Functions*, edited by M. Abramowitz and I. A. Stegun (Dover, New York, 1972).

[34] R. Wells, J. Quant. Spectrosc. Radiat. Transfer **62**, 29 (1999).

[35] D. D. S. Meneses, G. Gruener, M. Malki, and P. Echegut, J. Non-Cryst. Solids **351**, 124 (2005).

[36] J. Nocedal and S. J. Wright, *Numerical Optimization*, 2nd ed., Springer Series in Operations Research (Springer, Berlin, 2006).

[37] R. Pintelon and I. Kollár, IEEE Trans. Instrum. Meas. **54**, 318 (2005).

[38] S. I. Popova, T. S. Tolstykh, and V. T. Vorobev, Opt. Spectrosc. **33**, 444 (1972).

[39] T. S. Eriksson, A. Hjortsberg, G. A. Niklasson, and C. G. Granqvist, Appl. Opt. **20**, 2742 (1981).

[40] C. Koike, C. Kaito, T. Yamamoto, H. Shibai, S. Kimura, and H. Suto, Icarus **114**, 203 (1995).

[41] K. S. Kunz and R. J. Luebbers, *The Finite Difference Time Domain Method for Electromagnetics* (CRC Press, New York, 1993).

[42] K. Wakino, M. Murata, and H. Tamura, J. Am. Ceram. Soc. **69**, 1551 (1986).